Molecular Dynamics Simulation of a Glassy Polymer Surface

Kevin F. Mansfield† and Doros N. Theodorou*

Department of Chemical Engineering, University of California, Berkeley, and Center for Advanced Materials, Lawrence Berkeley Laboratory, Berkeley, California 94720

Received April 26, 1991; Revised Manuscript Received July 8, 1991

ABSTRACT: The free surface of glassy atactic polypropylene is studied by molecular dynamics computer simulation. A model film system exposed to vacuum on both sides is examined at a temperature 22 °C below the experimental glass transition temperature of the bulk polymer. The vinyl chains are represented as collections of backbone carbon atoms with united atom pendant methyl groups and explicit hydrogens. Bond lengths are held fixed, while bond angles are flexible. Simulations have been performed for durations of up to 400 ps and incorporate density profile dependent long-range contributions to the energy and stress. The spatial dependence of the short-time dynamical properties of the model film has been determined. Enhancements in the mean-squared displacement of atoms, in the orientational relaxation of backbone bonds, and in the rate of torsion angle fluctuations within a conformational state are observed near the free surface. One must penetrate into the film by approximately 15 Å from the extreme edge before observing a behavior in these dynamical features that resembles that of the bulk glassy polymer. This "dynamical interfacial thickness" is twice as large as the thickness over which the mass density profile varies. The center of mass motion of chains located as far as 2–3 times the unperturbed radius of gyration from the edge of the free surface is enhanced and highly anisotropic. Conformational transitions in the glassy polymer film have been analyzed. The glass is found to contain many "soft spots", where transitions occur with rates comparable to those observed in polymer liquids, as well as "stiff" regions, where the transitions are virtually arrested. An average rate for conformational isomerization in the polymer has been calculated by constructing a hazard plot of first passage times.

1. Introduction

Free surfaces of amorphous glassy polymers are encountered in a number of important technologies employing protective polymeric coatings, such as microelectronics. Typically one manipulates the wetting, friction, and wear characteristics of a surface by the use of different polymeric materials and/or processing conditions, so as to achieve acceptable performance for a given application.[1] Obtaining detailed microscopic-level information on the interfacial structure and mobility of a polymer, and establishing links between this information and overall thermodynamic and mechanical performance, could greatly aid in the improvement of existing polymeric coatings and the development of new ones. The goal of our work is to obtain such atomic-level information for a given polymer by statistical mechanics based computer simulation techniques, starting solely from a knowledge of the polymer's chemical constitution and interatomic interactions.

We recently reported our findings from a molecular mechanics (MM) computer simulation study of the glassy atactic polypropylene/vacuum interface at −40 °C (22 °C below the experimental glass transition temperature, T_g, of the bulk polymer).[2] The chains were represented in atomistic detail as assemblages of backbone carbons, pendant hydrogens, and pendant methyl groups. In that work, the model glass was viewed as locally fluctuating around static model microstates, each created by the MM technique. Each static model microstate was formed by minimizing the total potential energy of an initial guess configuration with respect to all microscopic degrees of freedom in a stagewise fashion. This procedure produced a collection of static model microstates, each "locked" within a local minimum of the potential energy in configuration space.[2,3] Averages taken over several such model microstates yielded predictions for the local structure at the free surface (e.g., density profile, bond orientation characteristics, torsion angle distribution, overall chain organization) as well as a theoretical estimate for the internal energy contribution to surface tension that agreed well with experiment.

The work reported here addresses the molecular mobility at a glassy polymer surface. A molecular dynamics (MD) computer simulation technique[4,5] has been employed to study the same glassy atactic polypropylene/vacuum interface as in our previous work. This technique allows for examining all dynamical processes with time scales less than the time duration of the simulation. The work reported here focuses only on the short-time (≤400 ps) dynamics of a glassy polymer free surface.

MD has been used to study many types of interfacial geometries such as vapor/liquid,[6–12] monolayer/solid,[13] and bulk liquid/solid interfaces.[14] Particular attention has been placed recently on studying fluids in confined geometries of molecular dimensions,[13,15–18] because of the relevance to industrial processes using membranes or microporous solid sorbents. In the past few years, there has been considerable interest in applying MD to macromolecular fluids.[19–29] Recently, Sylvester, Yip, and Argon[30,31] used MD to study the bulk properties of an atomistic model of atactic polypropylene. Their simulations were performed above and below T_g under conditions of constant pressure P and temperature T and yielded reasonable predictions of P–V–T properties, structural features that were in good agreement with X-ray scattering measurements and previous molecular mechanics simulations,[3] and characterizations of the unoccupied volume and its distribution. The work reported in this paper is the first to look at the *free surface* of an amorphous polymer in atomistic detail using molecular dynamics, thus providing new quantitative information on the local structure and mobility in such a system. To our knowledge, the only computer simulations performed so far on polymer/vacuum interfaces are our previous MM[2] and the Monte Carlo studies of Madden et al.[32,33]

* To whom correspondence should be addressed at the University of California.
† Present address: Air Products & Chemicals, Inc., 7201 Hamilton Blvd., Allentown, PA 18195.

0024-9297/91/2224-6283$02.50/0

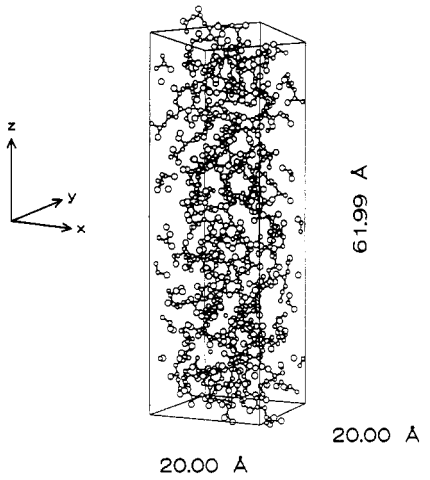

Figure 1. Snapshot of an atomistically detailed model microstate, composed of 12 parent chains of molecular weight 1110. The microstate is used to represent a thin film of glassy atactic polypropylene at a temperature of −40 °C. Vacuum is located at the top and bottom of the unit cell, and periodic boundary conditions are implemented in the x and y directions. The larger and smaller spheres correspond to methyls and backbone carbons, respectively. Pendant hydrogens have been omitted and van der Waals radii reduced for clarity.

The MD method and microscopic model used to represent our polymer/vacuum system are presented in section 2 of this paper. In section 3 we discuss the simulation strategy employed and its computational requirements. Next (section 4), simulation results are presented, followed by a summary and statement of conclusions drawn from this work (section 5). Finally, some mathematical details are elaborated in the appendices.

2. Model and Molecular Dynamics Method

The physical system we studied is the surface region of a thin film of glassy atactic polypropylene at −40 °C. This film is assumed sufficiently thick so as to contain a region far from any interfaces that behaves as bulk polymer in all aspects (structurally, dynamically, and thermodynamically). We model this system in a detailed microscopic manner, as in our previous MM work.[2] Local regions in the film are envisioned as fluctuating around configurations which constitute local minima of potential energy, and a realistic distribution of such minima is assumed to be provided by our MM method. The polymer is modeled as consisting of three types of interacting sites: backbone carbons (C), pendant hydrogens (H), and pendant methyl groups (CH_3 or R). The chains are viewed as monodisperse and linear, of the form $RCHR(CH_2CHR)_{x-1}R$. Each chain has a degree of polymerization of $x = 26$, corresponding to a molecular weight of 1110, $N = 155$ interaction sites, 52 skeletal bonds (including the two C–R bonds at each chain end), and 154 total bonds. The tacticity is Bernoullian with a fraction of meso diads $w_m = 0.48$.[2,3,30,31] The rotational isomeric state (RIS) model[34-36] value at −40 °C for the radius of gyration of our chains in the unperturbed state is $\langle s^2\rangle_0^{1/2} = 10.28 \pm 0.01$ Å. A model microstate, or unit cell, is constructed from $N_c = 12$ parent chains, placed within an orthorhombic box of dimensions $h_1 = 20$ Å, $h_2 = 20$ Å, and $h_3 = 61.99$ Å, as shown in Figure 1. Periodic boundary conditions[4] are implemented in the x and y directions, so that the system behaves as if infinite in these two directions.

The MD approach used here is an extension of the single-chain work of Sylvester et al. on bulk atactic polypropylene[30,31] to a multichain glassy atactic polypropylene/vacuum system. Nonbonded interatomic interactions are accounted for between all minimum image pairs of interacting sites using pairwise additive Lennard-Jones potentials $\mathcal{V}_{ij}^{NB}$ that have been truncated and smoothed to zero at $2.33\sigma_{ij}$ by a quintic spline.[2,3] A Verlet neighbor list[4] with a skin thickness of $0.2\sigma_{ij}$ was used in all calculations. Long-range attractions between atom pairs beyond the truncation distance are accounted for by integrated potential functions $\mathcal{V}_{ij}^{tails}$, which take into account the actual density profile of the film (see Appendix A). Bond lengths are held fixed by holonomic constraints implemented in the manner developed by Edberg, Evans, and Morriss.[37] Bond angles (bonded three-body interactions) are assumed flexible, since it has been shown[38] that constraining their values, and thereby eliminating the coupling between bond angle vibrational and bond torsional motion, results in a poor approximation of true dynamical behavior. A simple harmonic potential is used to keep an angle formed between three bonded atoms ijk near its equilibrium value θ^0_{ijk}:

$$\mathcal{V}_{ijk}^{BA} = C^{\theta}_{ijk}(\theta_{ijk} - \theta^0_{ijk})^2 \quad (1)$$

In addition, there is a 3-fold symmetric intrinsic torsional potential (four-body bonded interaction) $\mathcal{V}_{ijkl}^{\phi}$ associated with skeletal bonds.[2,3]

Potential parameters are taken primarily from our earlier MM work[2,3] and the MD simulations of Sylvester et al.[30] The intrinsic torsion angle potential was assigned a barrier height of 2.8 kcal/mol. The lengths of the C–H, C–C, and C–CH_3 bonds were 1.10, 1.53, and 1.53 Å, respectively.[2,3] Parameters for eq 1 were taken from the values reported by Sylvester et al. (ref 30, Table I). The only change in potential parameters relative to previous MM and MD work was introduced in the van der Waals radii r_i^0 of the interacting sites. We determined that an increase in the r_i^0 values for C, H, and CH_3 by 0.04 Å,[39] which is well within their experimental uncertainty,[40] was needed to yield the correct average bulk density of 0.892 g/cm^3 with our flexible dynamic model of atactic polypropylene in the presence of long-range energetics. The Lennard-Jones potential parameters corresponding to the adjusted r_i^0 values and previously used values for the atomic polarizabilities and effective numbers of electrons[3,36,40] are summarized in Table I.

Table I
Lennard-Jones Potential Parameter Values[3,36,40]

atom or group (i)	r_i^0,[a] Å	α_i,[b] Å^3	$N_{e,i}$,[c]	σ_{ii},[d] Å	ϵ_{ii}/k_B,[e] K
H	1.34	0.42	0.9	2.388	32.00
C	1.84	0.93	5.0	3.279	37.08
CH_3	2.04	1.77	7.0	3.635	62.02

[a] van der Waals radius. [b] Atomic polarizability. [c] Effective number of electrons. [d] Lennard-Jones collision diameter. [e] ϵ_{ii} is the Lennard-Jones well depth; k_B is the Boltzmann constant.

The equations of motion are derived from an exact Lagrangian using Cartesian coordinates of all atoms as the degrees of freedom, with the incorporation of holonomic constraints to conserve bond lengths. Our Lagrangian (eq 2), for the microcanonical ensemble, is defined as the

$$\mathcal{L} = \frac{1}{2}\sum_{i=1}^{N_cN} m_i \dot{r}_i^2 - \sum_{i<j}\mathcal{V}_{ij}^{NB} - \sum_{i<j}\mathcal{V}_{ij}^{tails} - \sum_{i<j<k}\mathcal{V}_{ijk}^{BA} - \sum_{i<j<k<l}\mathcal{V}_{ijkl}^{\phi} \quad (2)$$

difference between kinetic (first term) and potential energy (other terms).[41,42] In eq 2, $\mathcal{V}_{ij}^{tails}$ is summed over all atom pairs (see Appendix A) while $\mathcal{V}_{ij}^{NB}$ is summed only over minimum image nonbonded pairs of atoms. m_i is the mass of atom i. The $N_c(6x - 2)$ holonomic equations of

constraint, one for each constrained bond length between atoms i and j, take the form

$$g_l = (r_i - r_j)^2 - d_l^2 = 0 \tag{3}$$

where d_l is the fixed bond length.[37] The $3N \times N_c$ second-order differential equations of motion for the molecules in the system are obtained from eq 2 by[41,42]

$$\frac{d}{dt}\frac{\partial \mathcal{L}}{\partial \dot{q}_k} = \frac{\partial \mathcal{L}}{\partial q_k} + \sum_l \lambda_l \nabla_k g_l \tag{4}$$

q_k are the degrees of freedom, λ_l are the Lagrange undetermined multipliers associated with the constraints g_l, and the summation is taken over the constraints corresponding to those atoms (up to four) that are bonded to atom k. The entire term $\sum_l \lambda_l \nabla_k g_l$ is known as the constraint force and corresponds to the force applied to the degree of freedom k so as to satisfy the conditions of the constraints (eq 3). The λ's are found using the Gauss principle of least constraint.[37] This approach is very different from other iterative methods, such as SHAKE,[43] which have been commonly used in the past for bonded systems. The use of bond length constraints and the fact that our simulations conserve total linear momentum reduce the total number of independent degrees of freedom f (originally $3N \times N_c$) by the number of constraints and by 3, respectively. The correct f is required to determine the true temperature of the simulation from the kinetic energy.[4,5]

Polymer glasses are inherently configurationally arrested, characterized by immeasurably small chain self-diffusivities. An assumption of this work is that local regions in a polymer glass fluctuate around static model microstates, as was assumed in earlier MM studies.[2,3] We obtain most properties of our glassy model film by arithmetically averaging over many different model microstates rather than by simulating one structure for a very long time.

3. The Simulation

The MD computer simulation proceeds through a multistage strategy. The first stage is the generation of an initial configuration for all polymer chains in the form of a static model microstate through MM.[2] In summary, this procedure first "grows" several parent chains in a unit cell by a Monte Carlo scheme and then minimizes the total potential energy of the model microstate with respect to all microscopic degrees of freedom. The resulting microstates satisfy the conditions of detailed mechanical equilibrium; i.e., they reside in local minima of the potential energy hypersurface. The reader is referred to ref 2 for details. Five independently generated static model microstates were created in this manner and then subjected to dynamic simulation.

To start the dynamics, velocities are assigned to all interaction sites in a given static microstate from a Maxwell–Boltzmann distribution[4] at −40 °C. Next, a series of three consecutive MD runs are performed under different macroscopic constraints to efficiently equilibrate the microstate. The goal of the first equilibration run is to partition the kinetic energy among the system degrees of freedom, while preserving the desired simulation temperature. This is accomplished by running the simulation isothermally for a time duration of 15 ps, using the extended ensemble approach of Nosé and Hoover.[39,44-47] The second equilibration run, taking place between t = 15 ps and t = 45 ps, aims at producing a model microstate with an isotropic stress tensor throughout its middle region, here defined as the central one-third of the unit cell. The desired value of all components of the stress is zero. At the start of this run we begin to monitor the stress tensor and one-third its trace (the stress) in the middle region of the film following the Harasima convention.[2,9-12,39,48] Long-range contributions to the stress are included (see Appendix B). The average and variance of the stress tensor in the middle region are accumulated between t = 15 ps and t = 19 ps. Once the t = 19 ps mark is past, we start comparing the instantaneous value of the bulk stress at each time step to the preaccumulated 4-ps average. As soon as the instantaneous stress comes within 1 standard deviation of the average, the three edge lengths of the cell are adjusted by a Newton–Raphson step[49] aimed at driving the bulk stress to zero. This Newton–Raphson scheme employs numerically estimated derivatives of the stress with respect to the cell edge lengths. Upon rescaling the cell dimensions, all atomic coordinates are subjected to an affine transformation that leaves the box center invariant. After the box dimensions have been rescaled, the average stress accumulators are zeroed and the procedure of averaging the stress is restarted over a new 4-ps-long interval, after which the edge lengths are rescaled again. In all, the cell size is changed five times for each model microstate. After the fifth rescaling (around t = 35 ps) the MD continues under isothermal conditions until t = 45 ps. The third equilibration phase is a straightforward microcanonical MD simulation between t = 45 ps and t = 60 ps. This is followed by the 52-ps-long microcanonical production phase of the simulation, during which all structural, thermodynamic, and dynamical quantities of interest apart from conformational isomerization kinetics are monitored. "Extended ensemble" methods were avoided during the production phase, since the fictitious "masses" they require[50] (for whose choice no equivocal physical basis exists) have been shown to affect the dynamics. The standard deviation of the instantaneous temperature within a given production phase of a run was 3.93 K, while the average temperature over the five independent runs was 232.2 ± 4.4 K. The total normal stress in our films was quite small, a typical value over a single run being 10 ± 55 atm. (The uncertainty here was computed by block averaging with a statistical inefficiency factor of 10, corresponding to a correlation time of 0.1 ps.)[4]

The equations of motion were integrated by a fifth-order Gear predictor–corrector method, using only a single corrector step.[4] A variable, self-adjusting time step method was implemented, which ensured that the absolute deviation between predicted and corrected accelerations was less than 5×10^{-4} times the magnitude of the acceleration. The average time step was 0.4 fs, which is considerably smaller than in previous n-alkane work (ca. 2 fs).[20-29] This is because our simulation has to follow the high-frequency vibrational motions of H–C–H bond angles.[39]

A realistic representation of the dynamics of an anisotropic system demands explicit consideration of long-range forces. (This is not necessary in more conventional bulk-phase simulations, as long-range forces there are isotropic.) A scheme combining accuracy and computational tractability was developed for this purpose. Evaluating the long-range force on every atom requires a double loop over all pairs of atoms in the system (not only minimum image pairs) and is thus very computationally demanding. It was found that the contribution $\mathcal{V}_{ij}^{\text{tails}}$ makes to the total force on an atom, while large in magnitude, varies slowly with simulation time compared to all the other forces. To avoid excessive computations, and without significant loss in the conservation of the Hamiltonian, $\mathcal{V}_{ij}^{\text{tails}}$ was held constant over periods of 50 time steps and then updated based on the current positions of all atoms. A related

scheme for long-range corrections has been proposed recently by Tuckerman, Berne, and Martyna.[51] Numerical error associated with integrating the equations of motion results in slight violations of the bond length constraints, which grow slowly in time. This problem was corrected using the Edberg, Evans, and Morriss bond length Φ and velocity Ψ penalty functions (see eqs 12 and 13 of ref 37), which were monitored at each time step and minimized to 1×10^{-12} for individual chains whenever their Φ or Ψ exceeded 1×10^{-8} or 1×10^{-7}, respectively. This choice of tolerances ensured that discontinuities in the Hamiltonian and the total linear momentum brought about by the restoration of constraints were insignificant. The above-described algorithmic choices resulted in a model system Hamiltonian that is conserved to approximately five significant figures during the production phase of the simulations.

Atomic positions (in the primary unit cell) and velocities were written to disk every 10 fs during the equilibrated portion of the MD simulation for postprocessing.[4] No volatilization of the polymer occurred over the short-time duration of the simulations, as would certainly be observed if our system were a simple fluid.[6-12]

All computations were performed on the CRAY Y-MP8/864 located at the San Diego Supercomputer Center. Codes are written in FORTRAN and highly vectorized in order to take advantage of the pipelining capabilities of the machine. Our MD programs can simulate approximately 2.7 ps of motion per CPU hour.

4. Results

The five individual molecular dynamics simulations performed provided detailed information on the molecular structure, short-time dynamics, as well as several thermodynamic properties of the model glassy polymer/vacuum interface.[39] In this paper, emphasis is placed on spatially resolving the short-time molecular mobility in the film, characterized through several dynamical quantities. In analyzing our results, we partition each simulation box into 1-Å bins normal to the z axis. Findings are symmetrized with respect to the film midplane passing through the box center of mass, which thus reflects an arithmetic average over 10 half-model microstates. This method of superposing model microstates does not give special consideration to the fact that our five model films have somewhat different surface areas, as a result of the rescaling procedure used between $t = 15$ ps and $t = 45$ ps (see the previous section). The surface area of the five films was 393.2 ± 2.4 Å^2 (mean $\pm$ standard deviation), so neglecting its variation was judged legitimate. The glassy model films differ substantially from each other in configuration; therefore, the values obtained for the structural features and dynamical and thermodynamic properties vary substantially from film to film. The qualitative behavior of these results, however, is always the same across all films.

The local mass density profile is shown in Figure 2. In this figure, as well as those that follow, the film midplane lies at $z = 0$ Å and vacuum is present at the extreme right. The error bars represent the variance of the mean in each bin. For comparison, the experimental value of the bulk density of atactic polypropylene at −40 °C is also indicated, which agrees favorably with our simulation results for the bulk region of the film. Note that the bulk density is free to change in the dynamic simulation. The density profile at the surface is sigmoidal, as at the vapor/liquid interface of simple fluids.[6-12] No evidence for chain layering, observed in simulations of n-alkanes next to solid surfaces,[13-18,27] is seen. The shape of this profile suggests

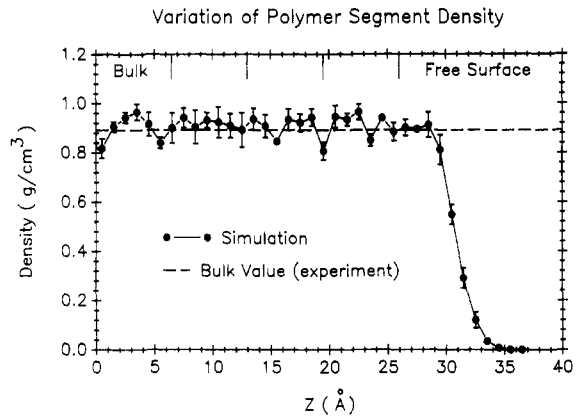

Figure 2. Local mass density distribution at a glassy atactic polypropylene/vacuum interface. The experimental bulk density is indicated by the dashed line. The short-time dynamical characteristics of the model film are spatially resolved by analyzing the results of the simulation separately in each one of five representative regions, ranging from "bulk" to "free surface". The five regions are defined by the tick marks indicated at the top of the figure.

an interfacial thickness of roughly 7 Å, in excellent agreement with the prediction from our previous MM study.[2] The slight maximum present in the molecular mechanics results (see Figure 5 of ref 2) is most probably a vestige of the initial guess generation procedure and goes away here when thermal motion is introduced. The profile obtained from MD provides a more accurate representation of reality. All other structural features, such as bond orientation, chain shape, and overall orientation, agree completely between these MD calculations and our earlier much less computationally demanding MM simulations and are not repeated here.

The spatial dependence of short-time mobility in the model film is analyzed by partitioning the microstates into five representative regions on each side of the midplane, as defined by the tick marks at the top of Figure 2. The four inner regions, which start at $z = 0$ Å and are each 6.5 Å thick, are characterized by a density that is indistinguishable from that of the bulk polymer. The outermost region, which starts at $z = 26$ Å, encompasses the entire remaining interfacial region. Local mobility has been characterized in each of these regions by accumulating several time autocorrelation functions as well as mean-squared displacements of atoms, chain centers of mass, and mean-squared angular displacements of torsion angles. To avoid processing highly correlated information, and at the same time take full advantage of the relatively limited degree of molecular motion present in our model glass, time origins in the computation of the time correlation functions[4] were chosen every 0.5 ps. Resolving the mean-squared displacements and autocorrelation functions spatially is accomplished by assigning each piece of dynamical information analyzed to one of the above-mentioned five regions of the film based on where the z coordinate of the atom (bond center, chain center of mass) resides at the time origin. At large time separations there is a chance for the atoms (bonds, centers of mass) to leave the bin to which they were assigned at the time origin. Given the low mobility of glassy polymers and the short time scales analyzed here, this possibility does not pose any serious problems.

One aspect of dynamics we investigated was the displacement of individual atoms and methyl groups on the chain. Given the frozen-in structure of glassy polymers, the short-time features of this motion cannot be associated with a chain self-diffusion, which is immeasurably slow in the glass. The picture we envision is one of atoms rattling

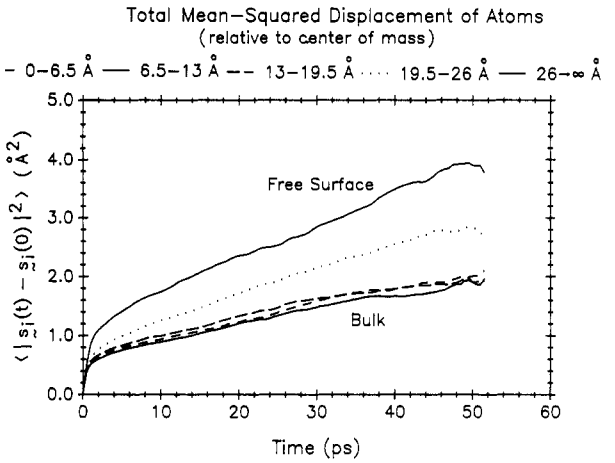

Figure 3. Mean-squared displacement of all atoms in the five representative regions of the model film indicated in Figure 2, as a function of time (eq 5). Any motion resulting from overall chain migration has been removed by subtracting from each atomic displacement the displacement of the center of mass of the chain to which it belongs.

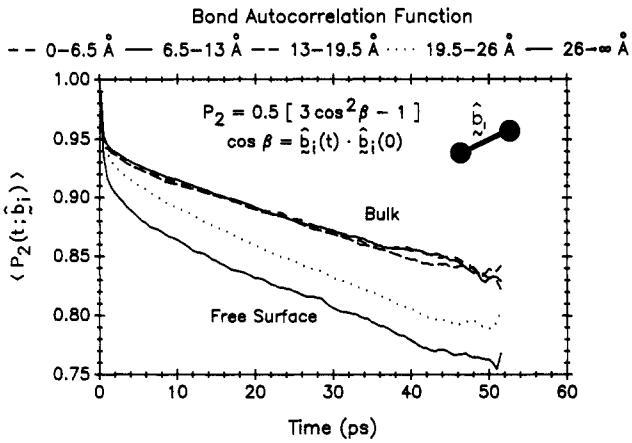

Figure 4. Time autocorrelation function of backbone bond vectors at different locations within the model film. $P_2(t;\hat{\mathbf{b}}_i)$ stands for the second-order Legendre polynomial of the first kind with argument $\hat{\mathbf{b}}_i(0)\cdot\hat{\mathbf{b}}_i(t)$, where $\hat{\mathbf{b}}_i$ is a unit vector along a backbone bond of a polymer chain. The result in each region has been averaged over all bonds whose midpoint lies within the region and over all model films simulated.

within small pockets of local free volume, with little chance of long-range motion (escape). One can characterize the fluctuation in chain shape resulting from such local motions by examining the displacement of atoms relative to the center of mass of the chain to which they belong. The mean-squared displacement relative to the chain center of mass is

$$\langle|\mathbf{s}_i(t)-\mathbf{s}_i(0)|^2\rangle_b = \frac{1}{N_b}\sum_{\alpha=1}^{3}\sum_{i=1}^{N_b}\{[r_{i,\alpha}(t)-\mathrm{com}_{i,\alpha}(t)]-[r_{i,\alpha}(0)-\mathrm{com}_{i,\alpha}(0)]\}^2 \quad (5)$$

In eq 5, α stands for a coordinate direction, $r_{i,\alpha}$ denotes the α-component of the position vector of atom i, and $\mathrm{com}_{i,\alpha}$ stands for the α-component of the center of mass position of the chain to which atom i belongs. N_b is the total number of atoms assigned to the considered bin. The quantity $\langle|\mathbf{s}_i(t)-\mathbf{s}_i(0)|\rangle_b$ is presented in Figure 3 for each of the five different regions of the film. The three middle regions ($z \leq 19.5$ Å, labeled "bulk") behave identically, which suggests that the middle region of the film is indistinguishable from bulk polymer as far as the dynamics of chain distortion are concerned. In addition, the long-time limiting slope of these curves is small, suggesting the absence of any long-range atomic diffusion. A significant enhancement in atomic mobility, compared to the glassy bulk, is observed in the two curves corresponding to the top two regions of the polymer. This important finding from Figure 3 implies that the motion of atoms around chain centers of mass does not reach its asymptotic bulk limit until one is approximately 15 Å from the extreme edge of the film. This thickness is by a factor of 2 larger than the distance over which the density, shown in Figure 2, departs from its bulk value. At the surface, the enhanced atomic mobility is a consequence of the lower density prevailing there. Apparently, the connectivity of chain segments enables this enhanced atomic-level mobility to propagate for some distance into the bulk. Chains that are exposed to the anisotropic surface region transmit dynamical information into the underlying polymer, even though the density there is indistinguishable from that of the glassy bulk. The individual components of $\langle|\mathbf{s}_i(t)-\mathbf{s}_i(0)|\rangle_b$ behave isotropically.[39]

The orientational relaxation of backbone carbon–carbon bonds was also analyzed by assigning a unit vector $\hat{\mathbf{b}}_i$ along each C–C bond as well as a second unit vector $\hat{\mathbf{d}}_i$ that is normal to each pair of adjacent skeletal bonds, originating at their common C atom.

$$\hat{\mathbf{b}}_i = \frac{\mathbf{r}_{i+1}-\mathbf{r}_i}{|\mathbf{r}_{i+1}-\mathbf{r}_i|}$$

$$\hat{\mathbf{d}}_i = \frac{\hat{\mathbf{b}}_{i+1}\times\hat{\mathbf{b}}_i}{|\hat{\mathbf{b}}_{i+1}\times\hat{\mathbf{b}}_i|} \quad (6)$$

$\hat{\mathbf{d}}_i$ is referred to as the out-of-plane vector by Weber and Helfand.[52] We follow the time evolution of these two types of vectors by constructing time autocorrelation functions in terms of the first (P_1) and second order (P_2) Legendre polynomials of the first kind

$$P_1(t;\hat{\mathbf{u}}_i) = \cos\beta$$

$$P_2(t;\hat{\mathbf{u}}_i) = \tfrac{1}{2}[3\cos^2\beta - 1] \quad (7)$$

where $\hat{\mathbf{u}}_i$ is equal to $\hat{\mathbf{b}}_i$ or $\hat{\mathbf{d}}_i$. In eq 7, $\cos\beta$ is calculated from $\hat{\mathbf{u}}_i$ by

$$\cos\beta = \hat{\mathbf{u}}_i(t)\cdot\hat{\mathbf{u}}_i(0) \quad (8)$$

$P_1(t;\hat{\mathbf{u}}_i)$ and $P_2(t;\hat{\mathbf{u}}_i)$ give a sense of the rate at which bonds lose memory of their orientation through thermal motion. By definition, $P_l(0;\hat{\mathbf{u}}_i) = 1$ whereas $\lim_{t\to\infty} P_l(t;\hat{\mathbf{u}}_i) = 0$ (where $l = 1, 2$). The local $P_2(t;\hat{\mathbf{b}}_i)$ is presented in Figure 4, averaged over all backbone bonds in a given bin. We do not see a full decay to zero for this property within the time scales studied in this work. This is expected, since Brownian dynamics simulations of an infinite molecular weight polymer solution, in which the overall molecular mobility is much larger than that in the glassy polymers studied here, have predicted the relaxation time of $P_1(t;\hat{\mathbf{b}}_i)$ to be longer than 1000 ps.[52] However, we can still examine differences in short-time mobility resulting from the presence of interfaces. In Figure 4, we find that bonds located near the free surface lose memory of their orientation significantly faster than those situated in the bulk. The local reorientational tendencies of the out-of-plane vectors are shown in Figure 5, represented in terms of the autocorrelation function $P_1(t;\hat{\mathbf{d}}_i)$. From these two figures, as well as from an analysis of the spatial dependence of $P_1(t;\hat{\mathbf{b}}_i)$ (result not shown),[39] we conclude that there is increased bond mobility at the surface compared to the bulk. The three regions in the film which are farthest

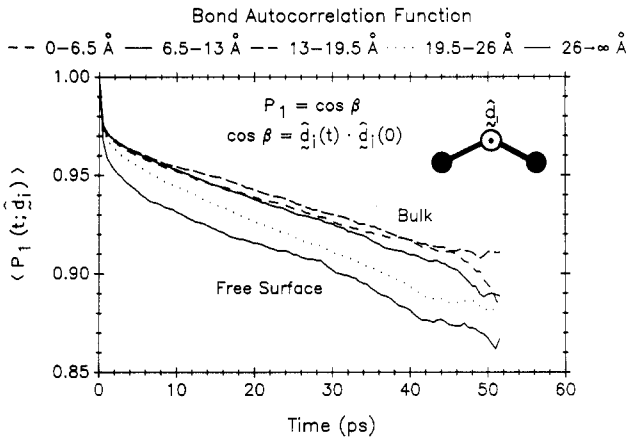

Figure 5. Spatial dependence of the time autocorrelation function for the out-of-plane vectors. $P_1(t;\hat{\mathbf{d}}_i)$ stands for the first-order Legendre polynomial of the first kind with argument $\hat{\mathbf{d}}_i(0)\cdot\hat{\mathbf{d}}_i(t)$. It measures the directional change of the $\hat{\mathbf{d}}_i$ vectors, which are unit vectors normal to neighboring pairs of backbone bonds, as shown in the inset.

Table II
Spatial Dependence of Bond Relaxation Times

bin	range, Å	τ_1, ps	τ_2, ps	τ_1/τ_2
1	0–6.5	1208	468	2.58
2	6.5–13	1068	458	2.33
3	13–19.5	1119	418	2.68
4	19.5–26	776	303	2.56
5	26 → ∞	729	304	2.40

from the vacuum phase exhibit identical dynamical behavior. From this result we conclude that reorientational motion becomes bulklike for bonds located approximately 15 Å from the edge of the film, the same distance arrived at through our earlier analysis of atomic mean-squared displacements. In all regions of the film, $P_1(t;\hat{\mathbf{d}}_i)$ was found to decay faster than $P_1(t;\hat{\mathbf{b}}_i)$. This is because, for significant motion of a single $\hat{\mathbf{b}}_i$ to occur, there must be rearrangement of a number of the nearby bonds, which is highly hindered in the glass. On the contrary, bonds can rock back and forth slightly without relying on a significant amount of local cooperativity.

Bond relaxation has been fit to an empirical Williams–Watts expression[53]

$$P_l(t;\hat{\mathbf{u}}_i) = \exp[-(t/\tau_l)^\beta] \tag{9}$$

where τ_l is the relaxation time of the l-order Legendre polynomial, and β is a factor accounting for deviation from Debye behavior. The short duration of our simulations does not permit accurate assessment of β, so it was set to unity. For the bulk region of the film (i.e., middle three bins), we calculated $\tau_1 = 1132 \pm 71$ ps and $\tau_2 = 448 \pm 27$ ps for $\hat{\mathbf{u}}_i = \hat{\mathbf{b}}_i$ by finding the limiting slopes of ln (P_1) and ln (P_2) versus time between 10 and 45 ps. These values can only be viewed as semiquantitative, due to the short time scales over which they were obtained and the limited number of independent model microstates involved. The Debye model predicts the ratio of τ_1/τ_2 to be equal to 3 for purely isotropic tumbling motion. Our ratio is lower, around 2.5. This agrees qualitatively with the values of 2.6 obtained from the n-octane MD simulations of Weber[54] and 2.2 from the polyethylene MD work of Takeuchi and Roe (based on out-of-plane vectors),[55] both reported at 27 °C. Spatially resolved bond relaxation times are summarized in Table II. The τ_1 and τ_2 relaxation times of bonds in bin 5, labeled "free surface" on the figures, are by approximately 50% shorter than those in the corresponding bulk, while their ratio remains virtually unchanged. Note that the bond relaxation times reported

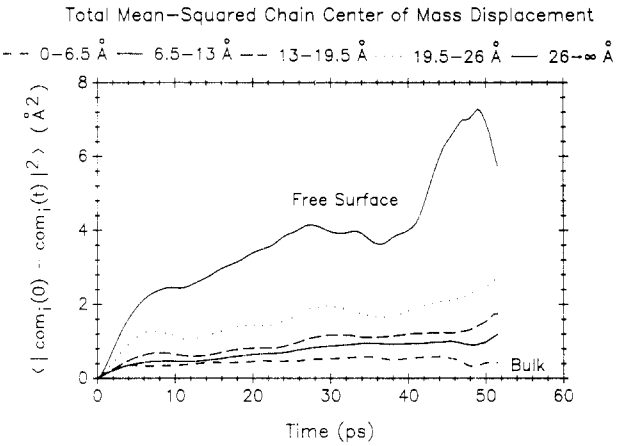

Figure 6. Total mean-squared displacement of chain centers of mass at various positions in the film. The film is partitioned into five regions or bins, as shown in Figure 2. Chains are assigned to the bin in which the z component of their center of mass resides. The free surface curve incorporates contributions from only four chains and is thus not as smooth as the rest of the data.

here are estimated from the near-linear regions of the time autocorrelation functions and that these same regions would probably show some remnants of initial short-time dynamical behavior if longer MD simulations were performed. This would have an effect of prolonging the relaxation times reported in Table II.

Dynamical behavior at a length scale associated with the overall chain motion has been examined by monitoring the mean-squared displacements of the chain centers of mass (Figure 6). Much longer MD runs would be required to safely calculate chain self-diffusivities from the limiting slopes of such plots; useful insight, however, can still be gained from a short-time analysis. The region closest to the midplane displays virtually no mobility, reflecting the truly locked in structure of a glassy polymer. The overall displacement of chains whose centers of mass are located in the free surface region is significantly enhanced compared to the bulk. (The error here is relatively large because only four chains contributed to the data.) This enhanced chain mobility, which becomes suppressed as one moves toward the bulk, appears to persist for about 30 Å (i.e., two to three $\langle s^2\rangle_0^{1/2}$) from the edge of the film, which is much larger than the 15-Å-thick region where we observed enhanced atomic and bond mobilities. Note that our chains are long enough to span the entire film thickness (end-to-end distance in the all-trans conformation = 66 Å). Another interesting result is that surface chains exhibit highly anisotropic center of mass motion, with displacements parallel to the surface being much greater than those normal to it. This result is consistent with the findings of an MD simulation of a simple liquid/vapor interface,[9] which were attributed to the anisotropic nature of the potential field exerted by neighboring molecules. This anisotropic motion can be clearly seen in Figure 7, where we display a yz projection of the 52-ps-long time trajectories of the 12 chain centers of mass located in a single model film. This motion slowly becomes more isotropic as the center of the film is approached, as indicated by the roughly spherical shape of trajectories near $z = 0$ Å. Chains with highly anisotropic motion, such as the one indicated by an arrow in Figure 7 (and shown more clearly in Figure 8), have a significant number of their segments in the surface region and are oriented such that their longest dimension is parallel to the surface. The anisotropic nature of center of mass motion persists for two to three unperturbed radii of gyration from the surface.

We now turn to dynamical characteristics associated with torsion angles. The features of interest explored in

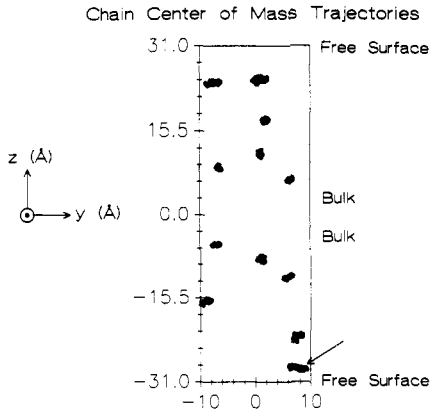

Figure 7. Chain center of mass trajectories in a single model microstate as obtained from a 52-ps-long MD production run. The projection of the center of mass trajectory onto the *yz* plane is shown for all 12 polymer chains contained in the chosen microstate. Dotted lines denote the regions over which the averages in Figure 6 were accumulated (compare regions in Figure 2). The anisotropic motion of chains located near the free surface is clearly demonstrated by the chain indicated with an arrow.

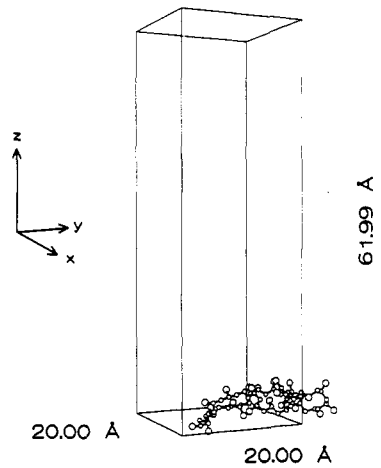

Figure 8. Conformation of a polymer chain that has its center of mass very near the edge of the polymer film. This chain is indicated with an arrow in Figure 7. All other surrounding chains have been removed, and the coordinates of the chain in question have been unfolded from the unit cell, for clarity.

this work include the following: (1) the distribution among conformational states; (2) the frequency and amplitude of torsion angle fluctuations within a given conformational state; (3) the rate of conformational transitions; (4) the mobility of torsion angles as a function of position along the backbone.

Each polymer chain used in this work has $2x - 2 = 50$ rotatable torsion (dihedral) angles. For consistency with our previous MM work,[2,3] we have numbered these angles along the chain as ϕ_2 to ϕ_{51}. The normalized equilibrium probability density of all angles in the film is shown in Figure 9. The assignment of angles follows the conventions of Theodorou, Suter, and Flory.[3,36] Perturbations in this distribution from the corresponding distribution of the bulk polymer, as a consequence of the presence of the two interfacial regions, have been shown to be mild (compare Figure 7 of ref 2). Therefore, Figure 9 represents the distribution of conformations in a bulk polymer and agrees well with previous MM work on bulk atactic polypropylene at the same temperature (compare Figure 6 of ref 3). The distribution obtained from MD is much smoother, however, due to the fact that we incorporate flexible bond angles and average over many more independent polymer configurations. The Suter and Flory RIS model[35,36] considers five rotational states for this polymer, located at −115° (ḡ), 15° (t), 50° (t*), 70° (g*), and 105° (g). We

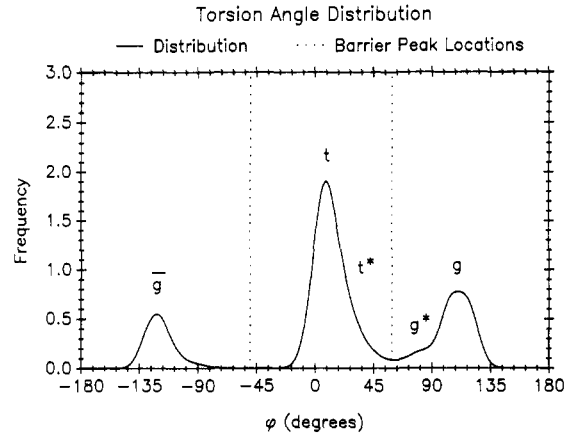

Figure 9. Distribution of skeletal bond torsion angles throughout the film. This result is practically identical to that seen in the bulk glassy polymer.[3] The dotted lines represent the locations of the potential energy barriers used in defining conformational states.

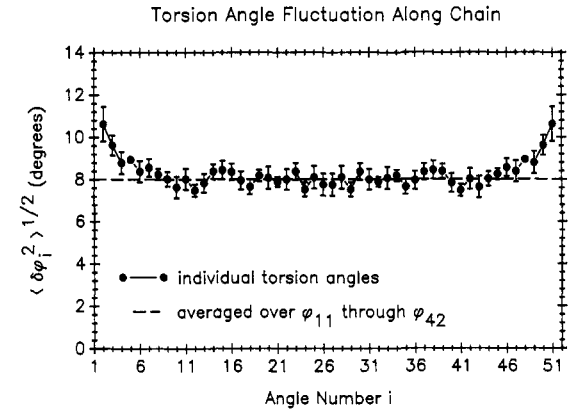

Figure 10. Standard deviation in torsion angles over 52 ps of simulation as a function of position along the backbone of the chain. ϕ_2 and ϕ_{51} lie closest to the chain ends. The dashed line represents the average fluctuation for ϕ_{11} through ϕ_{42}.

can clearly discern three of these states in Figure 9, namely ḡ, t, and g. The g* state appears as a shoulder peak to g, whereas the t* state is completely merged with t, giving rise to a skewness in the t peak. Our earlier MM work also showed some deviations between the locations and populations of torsional states and those predicted by the RIS method.[3]

The amplitude of torsion angle fluctuations was analyzed during the 52-ps production runs. The fluctuation of torsion angles was studied as a function of position along the chain. The variance of each ϕ_i was calculated individually and averaged over all chains in all five films. This resulted in a set of 50 variances (for $i = 2$–51), which were reduced to 25 by averaging over torsion angle pairs that reside at equal distances from the central segment of the chains. The standard deviation of torsion angles symmetrized in this way, $\langle \delta\phi_i^2 \rangle^{1/2}$, is displayed in Figure 10. The broken line represents the average standard deviation over the interior angles ϕ_{11} through ϕ_{42}. Clearly, the four or five torsion angles located near the ends of a chain are more mobile than interior angles. Turning a bond requires less cooperative motion near a chain end than near the middle of the chain. The same tendency for enhanced end mobility was detected in all regions of the film within the error of the simulation.

The rate of change in torsion angles has been examined by analyzing mean-squared angular displacements as a function of time. Mean-squared angular displacements are defined in a manner analogous to mean-squared displacements of centers of mass, discussed above. The

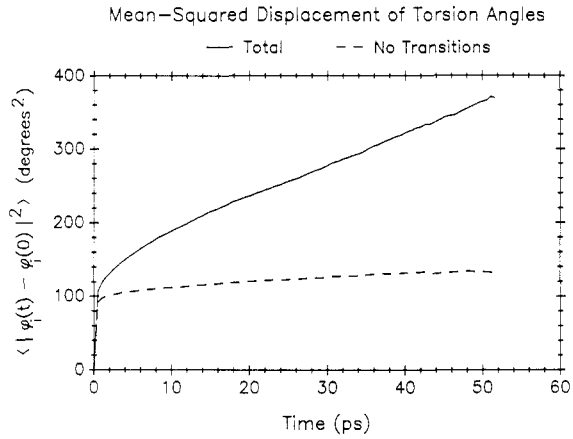

Figure 11. Mean-squared angular displacement of torsion angles with time in the glassy polymer film. The solid line shows the total mean-squared displacement and is heavily influenced by conformational transitions. The dashed line accounts only for angles that have not undergone a conformational transition during averaging. See text for details.

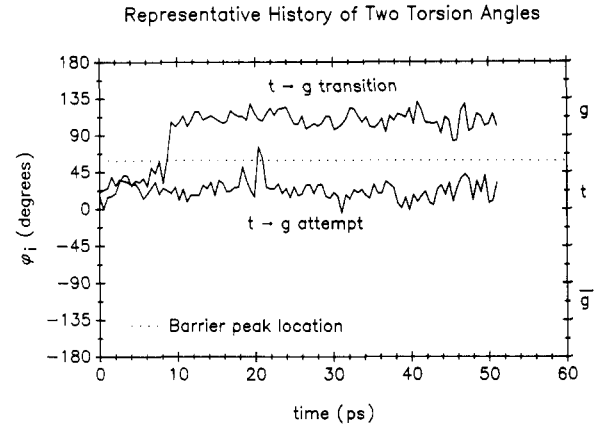

Figure 12. Evolution of the torsion angle for two skeletal bonds in one of the model systems simulated by MD. The potential energy barrier separating the t and g states is located at 59° (dotted line). One of the angles underwent a successful t → g transition at 90 ps. The other angle attempted a transition at 20 ps but quickly recrossed back into the t state.

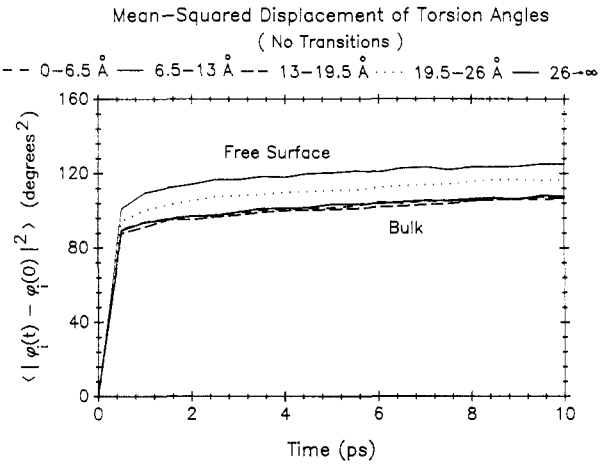

Figure 13. Spatial dependence of the mean-squared displacements of torsion angles in the model glassy polymer film. This result has only been averaged over those torsion angles which did not attempt or accomplish a conformational transition during the averaging (compare dotted curve on Figure 11).

result, averaged over all ϕ_i's in all systems, is presented in Figure 11 as a solid line. The mean-squared angular displacement quickly (in less than 10 ps) assumes a linear dependence on time which suggests that the way torsion angles change within the glass resembles a random-walk process. A similar linear behavior at long times has been detected in a MD simulation performed on liquid hexane by Clarke and Brown.[56] In that work, however, the mean-squared displacements of torsion angles exhibited a damped oscillatory behavior for times less than 1 ps, which is not observed in our system. Apparently, the torsional motion in our glassy polymer is almost completely chaotic, even for very short times. At very long times (i.e., several orders of magnitude longer than the times studied here) one expects the slope of the mean-squared angular displacement to asymptotically approach zero due to the fact that $\bar{g} \leftrightarrow g$ conformational transitions are virtually impossible. The mean-squared displacement of the torsion angles has also been analyzed spatially throughout the films, in the same five representative regions used previously. We observe virtually no systematic variation in this property as a function of position in the film. This method of characterizing bond angle motion is dominated by the few conformational transitions occurring in the glassy polymer, such as the $t \leftrightarrow g$ transition shown in Figure 12. In other words, when a torsion angle ϕ_i undergoes a conformational transition during the interval t, $|\phi_i(0) - \phi_i(t)|^2$ becomes very large. Just a few such transitions in a given region of the film can then significantly affect the slope of the mean-squared angular displacement (solid line in Figure 11) calculated for this region. Given the infrequent nature of conformational transitions (see below), any dynamical feature that is highly sensitive to them cannot be spatially resolved over a 52-ps-long run.

One can remove this dependence of the mean-squared displacement of torsion angles on conformational transitions by focusing selectively on those angles which are not involved in such transitions. The resulting mean-squared angular displacement reflects the torsional diffusion of angles within potential energy wells, rather than the process of overcoming torsional barriers. To study torsion angle motion in this way, we removed from the sampling all ϕ_i's which crossed the peaks of the potential energy barriers (see Figure 12) separating different conformational states at any time. In defining conformational transitions, only three states were considered, $\bar{g}$, t, and g; the barriers separating these states were taken at −50° and +59°, respectively (see Figure 9). No direct $\bar{g} \leftrightarrow g$ transitions were observed in any of the simulations, so consideration of a barrier between these two states is not necessary. Through this selection, our sample size was only reduced to 486.6 ± 10.1 ϕ_i's out of a total of 600 for a typical 52-ps-long run. The result for all angles is displayed in Figure 13 as a broken line. As expected, the long-time slope of this line is much lower than that of the continuous line on the same plot. This dynamical feature is resolved spatially over the different regions of the film in Figure 13 for times up to 10 ps. At 5 ps, the mean-squared displacement of the ϕ_i's located closest to the vacuum phase is by 19% larger than that of ϕ_i's in the center of the film. In addition, the three regions in the middle of the film are found to behave identically, indicating that the enhanced torsional motion at the surface persists for approximately 15 Å into the film.

The last dynamical aspect explored in our model glassy atactic polypropylene film was the rate and mechanism of conformational transitions. These radical changes in torsion angles across torsional barriers have been studied in detail for low molecular weight liquid *n*-alkanes, such as butane, by molecular dynamics and transition state theory based calculations.[54-60] The typical rate constant for conformational transitions in liquid butane at room temperature is approximately 65.0 ns^{-1} (i.e., on average each angle undergoes a transition roughly every 15 ps).[54,59,60] Randomly coiling polymers exhibit much lower

conformational transition rates, which have been investigated by Brownian dynamics[52,61-64] and in the recent MD work by Takeuchi and Roe.[55] In order to accumulate more meaningful information, we continued the MD simulation on one of the five model microstates for an additional 348 ps. This provided a 400-ps-long trajectory for conformational transition analysis. Results from this trajectory, although still relatively short on the time scales of interest and only representative of one glassy microstate, provided qualitative insight into the mechanism and rate of conformational transitions in glassy polymers.

Conformational transition rates have been calculated from computer simulations by several methods. Helfand, Wasserman, and Weber[52,54,61,62] have compiled first passage times and constructed hazard plots. Others have examined the decay of autocorrelation functions,[52,59,60] although these methods have been shown to require much longer simulation runs (by an order of magnitude) than hazard analyses.[52] Recently Brown and Clarke[60] calculated these rates from dihedral angle velocities. Here we estimate the overall conformational transition rate in two ways, by simply counting the number of successful transitions and by constructing a hazard plot.

The picture here is one of each torsion angle predominantly fluctuating in a given conformational state, and infrequently hopping to another state. Such hops are hindered by potential energy barriers, which in multichain systems arise from intramolecular and intermolecular interactions. We monitor successful transitions, as did Weber and Helfand,[52,54,61,62] by considering a transition of a torsion angle i to be complete only when ϕ_i has surmounted the peak of the potential energy barrier separating the two conformational states and reached the potential well bottom of the new state. Again we only consider a three-state model of the polymer ($\bar{g}$, t, g; see Figure 9). Transitions are located by examining every system configuration written to disk (one configuration every 10 fs), so that the fraction of missed transitions is small. This method of locating transitions, referred to as calculating first passage times, will still not completely account for all angles that recross the potential energy barriers; it is a significant improvement, however, over assuming that a transition takes place whenever a ϕ_i reaches the peak of the potential energy barrier. For example, 33 071 crossing of the barrier peak occurred during our 400-ps-long run, while only $N^{BC} = 242$ of these crossings succeeded in reaching the well bottom of the new conformational state. Still, approximately 60% of the angles contributing to N^{BC} recrossed the same potential barrier during some later time in the simulation. An estimate of the overall rate, k^{BC}, of well-to-well passages for our glassy polymer has been calculated by[55,56,60]

$$k^{BC} = N^{BC}/N_\phi t_{run} \qquad (10)$$

where $N_\phi = 600$ torsion angles and t_{run} is 0.400 ns. Using eq 10, we calculate $k^{BC} = 1.01$ ns^{-1} for this particular microstate of glassy atactic polypropylene at 233 K (which is an upper estimate due to the neglect of dynamical recrossing events, occurring when the torsion angle does not completely thermalize in the destination state). This k^{BC} is approximately by a factor of 60 smaller than that of liquid butane at 300 K. Unfortunately, the simulation was not long enough to resolve k^{BC} spatially. Conformational transition rates have been determined for individual ϕ_i's. The result for all 600 torsion angles, together with the average k^{BC} value, is presented in Figure 14. Individual angle transition rates range from zero to values almost as large as that encountered in n-butane at 300 K.[54,59,60] It is evident that dihedral angles with nonzero transition

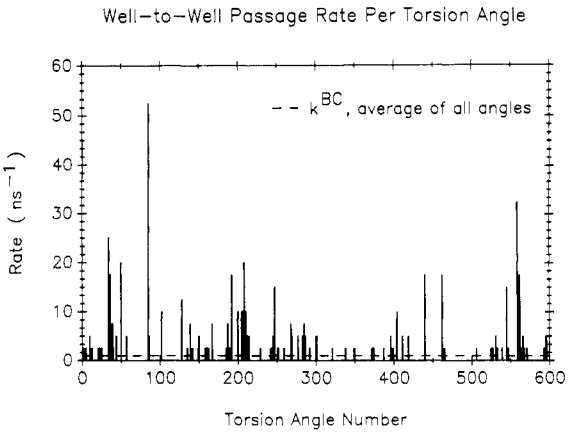

Figure 14. Individual conformational transition (well-to-well passage) rates for all torsion angles, calculated from a 400-ps-long MD simulation. The numbering convention used is such that angles 1–50 correspond to the first chain, 51–100 to the second chain, and so on. The average well-to-well passage rate k^{BC} (using eq 10) is indicated as a dashed line.

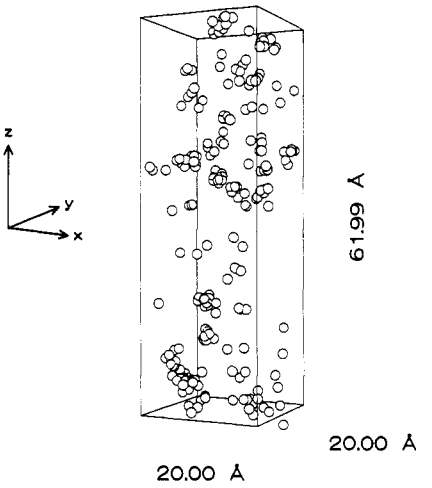

Figure 15. Spatial distribution of conformational transitions during a 400-ps-long MD run. Transitions are counted only when the minimum of the new state's potential energy well is reached. Each sphere corresponds to a C–C bond around which the transition has occurred and has a diameter equivalent to the C–C bond length (1.53 Å).

rates are grouped together along chains, implying some same-chain cooperatively in this type of motion. This finding is in qualitative agreement with the Brownian dynamics simulations of Helfand et al.[52,61,62] and the MD simulations of Takeuchi and Roe,[55] which showed high cooperativity between second-neighbor angles with the angle in-between in a trans state.

The coordinates of all bonds involved in the N^{BC} conformational transitions are plotted in Figure 15. Each sphere in this figure has a diameter equal to the C–C bond length and is centered at the center of the C–C bond at the new conformational state. In liquids and polymer melts, each torsion angle is equally susceptible to conformational transition (apart from deviations near chain ends). A different picture is conveyed by Figure 15 for the polymer glass. Here, approximately 90% of the spheres touch other spheres, forming clusters of high local mobility ("soft spots") separated by large, essentially transition-free ("stiff") regions. Some of the clustering results from the fact that the tendency to conformationally isomerize is correlated along the same chain (see Figure 14). In addition, strong intermolecular correlations between neighboring chains are observed in the soft spots. At the temperature of the simulation, soft spots do not percolate through the system; rather, there is a continuum of stiff

regions, in which conformational isomerization is inhibited by intermolecular packing effects.

A way of calculating the rate of conformational transitions which is perhaps more illuminating than the simple counting of eq 10 is the construction of hazard plots. The application of this technique to conformational isomerization in polymers is described in ref 62. The hazard rate $h(t)$ is defined such that $h(t)\,dt$ is the probability that a bond, which has not had a transition in a time t since its last transition, undergoes a transition (first passage) between t and $t + dt$. In other words, $h(t)$ is the instantaneous rate of first passages at time t.[65,66] For uncorrelated first passage times (Poisson process) this rate is a constant, λ. The cumulative hazard function is defined as

$$H(t) = \int_0^t h(t')\,dt' \tag{11}$$

For a Poisson process, $H(t)$ becomes λt and a plot of $H(t)$ versus t is linear. Such behavior has been seen at long times in Brownian dynamics simulations of polymer coils in solution.[62] Note, that the rate λ calculated from the long-time behavior of $H(t)$ is corrected for dynamical recrossing events, i.e., counts only transitions for which the bond has thermalized in the destination state. The cumulative distribution function $P(t)$ defines the probability that a transition will occur in a time less than t since the last transition:

$$P(t) = 1 - e^{-H(t)} \tag{12}$$

$P(t)$ is, of course, zero at $t = 0$ and approaches unity with increasing time. In our hazard plot construction, we have accounted for all angles that did not contribute a first passage time over the run by multiply censoring[66,67] our data. As is evident from Figure 14, 84.5% of the torsion angles did not undergo a transition during this simulation. Failure to take these into account would lead to the prediction of isomerization rates associated only with the mobile torsion angles, and not an overall rate. Here we censor the data associated with three characteristic times: (1) the times until the first transition of each angle since the beginning of the simulation production run (removal of first transitions);[62] (2) the entire simulation time for those angles which never underwent a transition; (3) the time between the last transition of each angle and the end of the run. The hazard plot is constructed by first arranging all time data (n values) in ascending order, including data that have been censored. The cumulative hazard corresponding to the mth time entry is then calculated from

$$\bar{H}_m = \sum_{l=1}^{m} \frac{1}{n + 1 - l} \tag{13}$$

where $m \leq n$. The summation in eq 13 takes place only over the uncensored data (see ref 67 for further details). Results are shown in Figure 16. The curved portion at short times is indicative of torsion angles which do not thermalize in the new conformational state and recross to their original states. The behavior at longer times is also nonlinear, suggesting that the underlying process whereby conformational transitions occur in the glass cannot be modeled as a Poisson process, as is the case for liquids and polymer melts. A physical reason for this could be that torsion angles in the stiff or locked-in regions of the glass are intrinsically much less susceptible to conformational isomerization than torsion angles within the soft spots. The curved nature of $H(t)$ implies that the instantaneous $h(t)$ is a not constant but rather a decreasing function of time. One can roughly divide the $H(t)$ plot into three

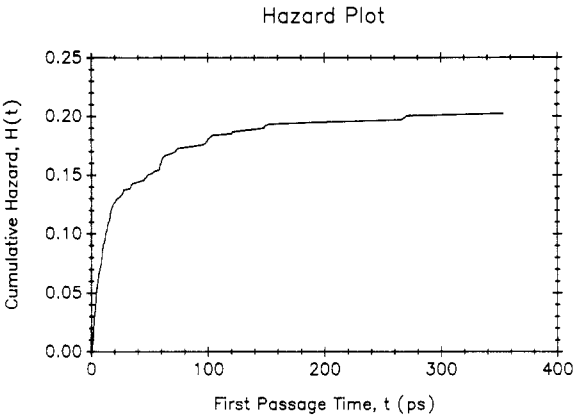

Figure 16. Hazard plot of first passage times for conformational transitions in a glassy polymer film. The cumulative hazard $H(t)$ is defined in eq 11 and calculated through eq 13. All torsion angles which do not undergo a conformational transition during the simulation are multiply censored (see text for details). For a Poisson process, the hazard plot would be a straight line.

regions. In the first one ($t < 30$ ps) the rate is strongly affected by fast recrossings of the barriers by bonds which have not completely thermalized in their destination state. The second one (30 ps $< t <$ 100 ps), with a slope of roughly 0.66 ns^{-1}, reflects the rate of conformational transitions of bonds in the mobile regions of the polymer glass. The third region ($t > 100$ ps) is strongly affected by bonds in the stiff domains of the polymer glass (compare Figure 15). The slope calculated from $H(t)$ between times of 150 and 350 ps is $\lambda = 0.054$ ns^{-1}. This limiting value of λ, as expected, is much lower than the value of k^{BC} calculated by simple transition counting (eq 10), since now highly mobile angles undergoing frequent transitions and recrossings are not contributing. Of course, it would take much longer simulations to establish whether the $H(t)$ plot becomes linear at long times for a polymer glass and to extract a conclusive rate constant λ for the process of conformational transitions.

5. Summary and Conclusions

Detailed molecular dynamics simulations have been performed on a free surface of glassy atactic polypropylene. An efficient equilibration strategy utilizing consecutive MD runs in different ensembles was employed to produce model microstates at the desired temperature and pressure that have isotropic stress tensors in their middle regions. Information on the structure and dynamics has been accumulated in the microcanonical ensemble from five 52-ps-long production runs on independently generated model films.

Structural features have been compared with earlier molecular mechanics work[2] on the same model system. Both simulations predict a sigmoidal density profile at the surface, which decays over a roughly 7-Å-thick region. The profile obtained through MD is slightly smoother. All other structural features are in quantitative agreement between the two methods. MM and MD require significantly different amounts of computational resources, however. For example, 20 static model microstates can be generated by MM in the time it takes to simulate the time evolution of a single glassy polymer configuration for 50 ps by MD.

Several dynamical properties of the model glassy polymer film have been examined. The atomic mobility is very low in the middle (bulk) region of the film. Atoms there remain virtually trapped in a frozen environment, only able to undergo very small scale motion. The presence of a polymer/vacuum boundary can significantly alter this

mobility. Enhancements in the mean-squared displacement of the atoms relative to the chain center of mass, in the rate of backbone bond orientational relaxation, and in the torsional diffusion of dihedral angles within rotational states were observed at the surface region compared to the bulk polymer. In many respects the free surface of our model glassy polymer behaves dynamically as a polymer melt. The above measures of local atomic mobility indicate that bulk glassy dynamical behavior is only exhibited by polymer located more than 15 Å from the extreme edge of the film. This "dynamical" measure of the interfacial thickness is approximately twice as large as the "static" thickness estimated on the basis of the density profile. The difference is explained by the fact that segments exposed to the attenuated surface region transmit dynamical information through bonds into the underlying layers of the polymer.

Chain center of mass motion has also been examined. Over the duration of the simulation the chains are very sluggish, as expected. Chains located a distance of less than 2–3 times the unperturbed radius of gyration (20–30 Å) from the extreme edge of the film are more mobile than those in the bulk. Thus one can define a third interfacial thickness based on the overall motion of chains, which is even larger than the dynamical thickness determined from atomic and bond motion. Clearly, interfacial thickness depends on the method of characterization employed, and this may have important implications for experimental measurements in this area. The motion of chain centers of mass located near the surface is highly anisotropic, being much more pronounced parallel than perpendicular to the free surface.

A final dynamical property examined was the rate of conformational transitions over a single 400-ps-long production run. We found our glassy film to possess local regions with liquidlike isomerization rates (soft spots) and stiff regions where conformational transitions were severely inhibited. This is in contrast to what happens in a polymer melt, where conformational transitions occur with equal probability throughout the polymer. The underlying mechanism of transitions has been examined through hazard analysis. This analysis indicates that conformational isomerization in glassy polymers cannot be viewed as a Poisson process. The observed transitions tend to be correlated between torsion angles on the same chain (particularly second-neighbor angles), as well as between angles on different chains but situated in the same vicinity of the glass. The overall rate of first passages between minima of the torsional potential in glassy atactic polypropylene at −40 °C (from eq 10) was found to be $\sim 1\ \mathrm{ns}^{-1}$. The effect of the presence of interfaces on this rate has not been quantitatively established.

Acknowledgment. We are grateful to M. Sylvester, S. Yip, and A. S. Argon for supplying us with a version of their bulk polymer computer code as well as for stimulating discussions. Financial support for K.F.M. was provided by the Director, Office of Energy Research, Office of Basic Energy Sciences, Materials Science Division of the U.S. Department of Energy under Contract No. DE-AC03-76SF00098. We thank the San Diego Supercomputer Center for generous amounts of computer time. Computational resources were also made available through gifts from E. I. du Pont de Nemours & Co. and B.P. America. D.N.T. expresses gratitude to the National Science Foundation for a 1988 Presidential Young Investigator Award, No. DMR-8857659.

Appendix A. Derivation of Long-Range Polymer/Polymer Interatomic Interaction Potential for Nonuniform Density Profiles

The short-range contribution to polymer/polymer interactions in our model film is accounted for by $\sum_{ij}\mathcal{V}_{ij}^{\mathrm{NB}}$ in eq 2, an explicit sum over all minimum image site pairs ij. $\mathcal{V}_{ij}^{\mathrm{NB}}$ is a modification of $\mathcal{V}_{ij}^{\mathrm{LJ}}$ that has been truncated and smoothed to zero between $R_{1,ij}$ and R_{ij}, by use of a quintic spline.[3] To account for the cohesive forces within the polymer film, we must include the long-range "tail" contribution as well.[68] This contribution corrects for interactions which have been represented by the spline part of $\mathcal{V}_{ij}^{\mathrm{NB}}$, rather than the full $\mathcal{V}_{ij}^{\mathrm{LJ}}$; in addition, it includes all atoms out to infinite distances which had no contribution to $\mathcal{V}_{ij}^{\mathrm{NB}}$. Failure to consider tails when integrating the equations of motion would lead to a decrease in the bulk density and an artificial distortion of the surface density profile. For the calculation to be self-consistent, the tail contribution must be obtained from the actual configuration of the model microstate, which fluctuates during the MD run.

Consider an atom pair ij in the unit cell and the long-range contribution from this pair to the potential energy $\mathcal{V}_{ij}^{\mathrm{tails}}$ in eq 2. We need to calculate the long-range energy that atom i experiences directly from all images of j, including the minimum image:

$$\mathcal{V}_{ij}^{\mathrm{tails}} = \sum_{j',\ \text{all images of } j} (\mathcal{V}_{ij'}^{\mathrm{LJ}} - \mathcal{V}_{ij'}^{\mathrm{NB}}) \qquad \text{(A.1)}$$

To do this we "smear" all images of j in two dimensions parallel to the xy plane within a slice of thickness δ. The atomic density in the slice is $2/\underline{a}\delta$, where $\underline{a}$ is the total surface area on both sides. The long-range energy due to the pair ij is

$$\mathcal{V}_{ij}^{\mathrm{tails}} = \mathcal{V}_{ij}^{\mathrm{tails}}(r_1{=}R_{1,ij};r_2{=}R_{ij}) + \mathcal{V}_{ij}^{\mathrm{tails}}(r_1{=}R_{ij};r_2{=}\infty) \qquad \text{(A.2)}$$

where

$$\mathcal{V}_{ij}^{\mathrm{tails}}(r_1;r_2) = \int_{z_j}^{z_j+\delta} \mathrm{d}z \int_{\rho_1}^{\rho_2} \rho\, \mathrm{d}\rho \int_0^{2\pi} \mathrm{d}\phi\, \frac{2}{\underline{a}\delta} \mathcal{V}_{ij}(r) \qquad \text{(A.3)}$$

In eq A.3, ρ is the radial distance of the smeared images of j from the projection of i on their plane, $\rho_1 = \{\max([r_1^2 - (r_{j,z} - r_{i,z})^2], 0)\}^{1/2}$, $\rho_2 = \{\max([r_2^2 - (r_{j,z} - r_{i,z})^2], 0)\}^{1/2}$, and $\mathcal{V}_{ij}(r) = \mathcal{V}_{ij}^{\mathrm{LJ}}(r) - \mathcal{V}_{ij}^{\mathrm{NB}}(r)$. The symbols r_1 and r_2 stand for two distances such that $r_2 > r_1$. A pictorial representation of these quantities is given in Figure 16 of ref 2.

With our frame of reference, $\mathcal{V}_{ij}^{\mathrm{tails}}$ only contributes to the z component of the forces on atom i. In other words, $F_{ij,x}^{\mathrm{tails}} = F_{ij,y}^{\mathrm{tails}} = 0$, and

$$F_{ij,z}^{\mathrm{tails}} = -\frac{\partial \mathcal{V}_{ij}^{\mathrm{tails}}}{\partial |\mathbf{r}_i - \mathbf{r}_j|} \frac{r_{i,z} - r_{j,z}}{|\mathbf{r}_i - \mathbf{r}_j|} \qquad \text{(A.4)}$$

The tail contribution to the diagonal elements of the stress tensor is derived by envisioning that all atom coordinates are scaled by the cell axes and using the analysis of Nosé and Klein[69]

$$\tau_{\alpha,\alpha}^{\mathrm{tails}} = \frac{h_\alpha}{h_1 h_2 h_3} \left\langle \sum_{i<j} \frac{\partial \mathcal{V}_{ij}^{\mathrm{tails}}}{\partial h_\alpha} \right\rangle \qquad \text{(A.5)}$$

The result for $\alpha = x$ or y is

$$\tau_{\alpha,\alpha}^{\mathrm{tails}} = \frac{\langle -\sum_{i<j} \mathcal{V}_{ij}^{\mathrm{tails}} \rangle}{h_1 h_2 h_3} \qquad \text{(A.6)}$$

and

$$\tau_{z,z}^{\text{tails}} = \frac{\langle -\sum_{ij} F_{ij,z}^{\text{tails}}(r_{i,z} - r_{j,z})\rangle}{h_1 h_2 h_3} \quad \text{(A.7)}$$

Equations A.6 and A.7 agree exactly with our previously derived result from direct integration.[2]

Appendix B. Alternative Expression for Stress Which Includes Long-Range Interactions

Recently we reported a new formulation for the internal stress tensor cast in terms of nonbonded interchain forces only.[2] Here we extend this idea to include long-range "tail" contributions to the stress for a system whose surface is exposed to vacuum (i.e., subject to a normal stress of zero). We start with eq F.1 of ref 2:

$$\tau_{\alpha,\alpha} = \frac{1}{\underline{V}}\langle \sum_{i\in\text{box}} r_{i,\alpha}^{\text{P}} \{ \sum_{j\in\text{box}} F_{ij,\alpha}^{\text{NB,min}} \}\rangle - \frac{1}{2\underline{V}}\langle \sum_{i\in\text{box}} \sum_{j\in\text{box}} (r_{i,\alpha} - r_{j,\alpha})_{\min} F_{ij,\alpha}^{\text{NB,min}}\rangle \quad \text{(B.1)}$$

The sums are taken over all pairs $i,j_{\min}(i)$ which belong to different images of the same parent chain or correspond to completely different parent chains. $\underline{V}$ in this case is simply $h_1h_2h_3$, and $r_{i,\alpha}^{\text{P}}$ stands for the α-component of the position vector of the parent chain image of atom i. Only the diagonal elements of the stress tensor have long-range contributions. We have extended eq B.1 so as to include all images of j and found the result to be[39]

$$\tau_{\alpha,\alpha}^{\text{tails}} = \frac{1}{\underline{V}}\langle \sum_{i\in\text{box}} r_{i,\alpha}^{\text{P}} \{ \sum_{j\in\text{box}} F_{ij,\alpha}^{\text{tails}} \}\rangle - \frac{1}{2\underline{V}}\langle \sum_{i\in\text{box}} \sum_{j\in\text{box}} (r_{i,\alpha} - r_{j,\alpha}) F_{ij,\alpha}^{\text{tails}}\rangle \quad \text{(B.2)}$$

Given that there is no total long-range contribution to the force in the x or y directions, as discussed in Appendix A, we can drop the first term of eq B.2 for $\alpha = x$ or y. The second term incorporates the tail contribution to stress in these two directions. While the tail contribution to the force in the z direction is nonzero, we note that $r_{i,z} - r_{j,z}$ is equal to $r_{i,z}^{\text{P}} - r_{j,z}^{\text{P}}$, due to the fact that there is no periodic continuation in this direction. Consequently, the two terms in eq B.2 cancel and offer no tail contribution to τ_{zz}.

References and Notes

(1) Wu, S. *Polymer Interface and Adhesion*; Marcel Dekker: New York, 1982.
(2) Mansfield, K. F.; Theodorou, D. N. *Macromolecules* **1990**, *23*, 4430.
(3) Theodorou, D. N.; Suter, U. W. *Macromolecules* **1985**, *18*, 1467; **1986**, *19*, 139; **1986**, *19*, 379.
(4) Allen, M. P.; Tildesley, D. J. *Computer Simulation of Liquids*; Clarendon Press: Oxford, 1987.
(5) Hansen, J. P.; McDonald, I. R. *Theory of Simple Liquids*, 2nd ed.; Academic Press: London, 1986.
(6) Rowlinson, J. S.; Widom, B. *Molecular Theory of Capillarity*; Oxford University Press: Oxford, 1989.
(7) Abraham, F. F.; Schreiber, D. E.; Barker, J. A. *J. Chem. Phys.* **1975**, *62*, 1958.
(8) Chapela, G. A.; Saville, G.; Thompson, S. M.; Rowlinson, J. S. *J. Chem. Soc., Faraday Trans. 2* **1977**, *73*, 1133.
(9) Eggebrecht, J.; Thompson, S. M.; Gubbins, K. E. *J. Chem. Phys.* **1987**, *86*, 2299.
(10) Rao, M.; Levesque, D. *J. Chem. Phys.* **1976**, *65*, 3233. Rao, M.; Berne, B. J. *Mol. Phys.* **1979**, *37*, 455.
(11) Nijmeijer, M. J. P.; Bakker, A. F.; Bruin, C.; Sikkenk, J. H. *J. Chem. Phys.* **1988**, *89*, 3789.
(12) Walton, J. P. R. B.; Tildesley, D. J.; Rowlinson, J. S.; Henderson, J. R. *Mol. Phys.* **1983**, *48*, 1357.
(13) Nicholson, D.; Parsonage, N. G. *Computer Simulation and the Statistical Mechanics of Adsorption*; Academic Press: London, 1982.
(14) Lupkowski, M.; van Swol, F. *J. Chem. Phys.* **1990**, *93*, 737.
(15) Magda, J. J.; Tirrell, M.; Davis, H. T. *J. Chem. Phys.* **1985**, *83*, 1888.
(16) MacElroy, J. M. D.; Suh, S. H. *Mol. Sim.* **1989**, *2*, 313; *Mol. Phys.* **1987**, *60*, 475.
(17) Schoen, M.; Cushman, J. H.; Diestler, D. J.; Rhykerd, C. L. *J. Chem. Phys.* **1988**, *88*, 1394.
(18) Peterson, B. K.; Gubbins, K. E.; Heffelfinger, G. S.; Marconi, U. M. B.; van Swol, F. *J. Chem. Phys.* **1988**, *88*, 6487.
(19) *Computer Simulation of Polymers*; Roe, R. J., Ed.; Prentice Hall: Englewood Cliffs, NJ, 1991.
(20) Rigby, D.; Roe, R. J. *Macromolecules* **1990**, *23*, 5312; **1989**, *22*, 2259; *J. Chem. Phys.* **1988**, *89*, 5280; **1987**, *87*, 7285.
(21) Kremer, K.; Grest, G. S. *J. Chem. Phys.* **1990**, *92*, 5057.
(22) Clarke, J. H. R.; Brown, D. *Mol. Sim.* **1989**, *3*, 27.
(23) Weber, T. A.; Helfand, E. *J. Chem. Phys.* **1979**, *71*, 4760.
(24) Ryckaert, J. P. *Mol. Phys.* **1985**, *55*, 549.
(25) Gao, J.; Weiner, J. H. *J. Chem. Phys.* **1989**, *91*, 3168.
(26) Gao, J.; Weiner, J. H. *J. Chem. Phys.* **1989**, *90*, 6749.
(27) Bitsanis, I.; Hadziioannou, G. *J. Chem. Phys.* **1990**, *92*, 3827.
(28) Murat, M.; Grest, G. S. *Macromolecules* **1989**, *22*, 4054.
(29) Hautman, J.; Klein, M. L. *J. Chem. Phys.* **1990**, *93*, 7483; **1989**, *91*, 4994.
(30) Sylvester, M. F.; Yip, S.; Argon, A. S. In *Computer Simulation of Polymers*; Roe, R. J., Ed.; Prentice Hall: Englewood Cliffs, NJ, 1991; pp 105–121.
(31) Sylvester, M. F.; Yip, S.; Argon, A. S. *Polym. Prepr. (Am. Chem. Soc., Div. Polym. Chem.)* **1989**, *30* (2), 32.
(32) Madden, W. G. *J. Chem. Phys.* **1987**, *87*, 1405.
(33) Lastoskie, C. M.; Madden, W. G. In *Computer Simulation of Polymers*; Roe, R. J., Ed.; Prentice Hall: Englewood Cliffs, NJ, 1991; pp 233–254; *Polym. Prepr. (Am. Chem. Soc., Div. Polym. Chem.)* **1989**, *30* (2), 39.
(34) Flory, J. P. *Statistical Mechanics of Chain Molecules*; Interscience Publishers: New York, 1969.
(35) Flory, J. P. *Macromolecules* **1974**, *7*, 381.
(36) Suter, U. W.; Flory, P. J. *Macromolecules* **1975**, *8*, 765.
(37) Edberg, R.; Evans, D. J.; Morriss, G. P. *J. Chem. Phys.* **1986**, *84*, 6933.
(38) van Gunsteren, W. F.; Karplus, M. *Macromolecules* **1982**, *15*, 1528.
(39) Mansfield, K. F. Ph.D. Dissertation, University of California at Berkeley, April 1991.
(40) Bondi, A. *Physical Properties of Molecular Crystals, Liquids and Glasses*; Wiley: New York, 1968.
(41) Goldstein, H. *Classical Mechanics*; Addison-Wesley Publishing Co.: Reading, MA, 1980; Chapter 2.
(42) Ciccotti, G.; Ryckaert, J. P. *Comput. Phys. Rep.* **1986**, *4*, 345.
(43) Ryckaert, J. P.; Ciccotti, G.; Berendsen, H. J. C. *J. Comput. Phys.* **1977**, *23*, 327.
(44) Nosé, S. *Mol. Phys.* **1984**, *52*, 255.
(45) Nosé, S. *J. Chem. Phys.* **1984**, *81*, 511.
(46) Nosé, S. *Mol. Phys.* **1986**, *57*, 187.
(47) Hoover, W. G. *Phys. Rev. A* **1985**, *31*, 1695.
(48) Ono, S.; Kondo, S. In *Encyclopedia of Physics*; Flügge, S., Ed.; Springer: Berlin, 1960; Vol. 10, p 134.
(49) Press, W. H.; Flannery, B. P.; Teukolsky, S. A.; Vetterling, W. T. *Numerical Recipes*; Cambridge University Press: Cambridge, 1986; Chapter 9.
(50) Kabadi, V. N.; Steele, W. A. *Mol. Sim.* **1990**, *4*, 371.
(51) Tuckerman, M. E.; Berne, B. J.; Martyna, G. J. *J. Chem. Phys.* **1991**, *94*, 6811.
(52) Weber, T. A.; Helfand, E. *J. Phys. Chem.* **1983**, *87*, 2881.
(53) Bahar, I.; Erman, B.; Monnerie, L. *Macromolecules* **1989**, *22*, 431.
(54) Weber, T. A. *J. Chem. Phys.* **1979**, *70*, 4277; **1978**, *69*, 2347.
(55) Takeuchi, H.; Roe, R. J. *J. Chem. Phys.* **1991**, *94*, 7446, 7458.
(56) Clarke, J. H. R.; Brown, D. *Mol. Phys.* **1986**, *58*, 815.
(57) Chandler, D. *J. Chem. Phys.* **1978**, *68*, 2959.
(58) Rosenberg, R. O.; Berne, B. J.; Chandler, D. *Chem. Phys. Lett.* **1980**, *75*, 162.
(59) Edberg, R.; Evans, D. J.; Morriss, G. P. *J. Chem. Phys.* **1987**, *87*, 5700.
(60) Brown, D.; Clarke, J. H. R. *J. Chem. Phys.* **1990**, *93*, 4117; **1990**, *92*, 3062.
(61) Helfand, E. *J. Polym. Sci., Polym. Symp.* **1985**, *73*, 39.
(62) Helfand, E.; Wasserman, Z. R.; Weber, T. A. *Macromolecules* **1980**, *13*, 526.
(63) Pear, M. R.; Weiner, J. H. *J. Chem. Phys.* **1979**, *71*, 212; **1980**, *72*, 3939.
(64) Fixman, M. *J. Chem. Phys.* **1978**, *69*, 1527, 1538.
(65) Helfand, E. *J. Chem. Phys.* **1978**, *69*, 1010.
(66) Bury, K. V. *Statistical Models in Applied Science*; Wiley: New York, 1975.
(67) Nelson, W. *J. Qual. Technol.* **1969**, *1*, 27.
(68) Mansfield, K. F.; Theodorou, D. N. *Macromolecules* **1991**, *24*, 4295–4309.
(69) Nosé, S.; Klein, M. L. *Mol. Phys.* **1983**, *50*, 1055.

Registry No. Polypropylene, 9003-07-0.